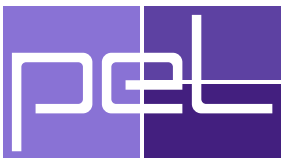

IEEE Transactions on Industrial Electronics, 64, no., pp. 4372–4381, Jun. 2017

Dynamic Assessment of Source - Load Interactions in Marine MVDC Distribution

U. Javaid, F. D. Freijedo, D. Dujic, *et al.*

POWER ELECTRONICS LABORATORY
ÉCOLE POLYTECHNIQUE FÉDÉRALE DE LAUSANNE

Dynamic Assessment of Source–Load Interactions in Marine MVDC Distribution

Uzair Javaid, *Student Member, IEEE*, Francisco D. Freijedo, *Senior Member, IEEE*, Drazen Dujic, *Senior Member, IEEE*, and Wim van der Merwe, *Senior Member, IEEE*

***Abstract*—Medium-voltage direct-current (MVDC) distribution is a possible replacement due to the advancements in power electronic technologies, for existing medium-voltage ac distribution on ships. The new systems based on MVDC are expected to increase fuel efficiency, remove bulky low-frequency transformers used for voltage coordination, and integrate storage technologies. These expected benefits of MVDC come with challenges such as stability and reliability of the new distribution system. In this paper, the effect of three different source-side converters, based on commercially available technology, on the MVDC distribution grid and their interactions with the constant power loads (propulsion drives) are investigated. Additionally, the effect of variations in the filtering effort and the distribution lengths on the system stability is analyzed using the impedance-based stability assessment.**

***Index Terms*—Impedance-based stability, medium-voltage direct-current (MVDC) systems.**

I. Introduction

AVAILABILITY of improved power electronic technologies, especially for the propulsion systems, has opened up opportunities to consider the medium-voltage direct-current (MVDC) electrical distribution as a possible replacement of the current medium-voltage alternating-current (MVAC) electrical distribution for the large ship on-board power systems. Guidelines concerning the new MVDC electrical distribution system have been outlined in [1]. Literature highlighting the viability of the future MVDC electrical distribution system, considering military and commercial vessels, has been published [2]–[11]. The advantages of MVDC electrical distribution, for ship on-board power systems, arise from the opportunities it provides in fuel efficiency, weight and space saving, and the flexibility in design of the system [12], [13].

All these advantages come with challenges, one of them being the lack of commercial MVDC equipment that can, nowadays, replace the existing MVAC components. To utilize the maximum benefit from the MVDC distribution system, improvements are required in the existing medium-voltage drives, high-voltage electrical machines, diesel engines and gas turbines, high-power dc–dc converters, rectifiers, MVDC protection components, MVDC cable technology, active and passive filters, and energy storage systems [14].

Another major challenge is the stability of the MVDC distribution system that arises due to the presence of the high-power motor drives and their constant power load (CPL) behavior [15]. These stability-related problems and their possible solutions can also be found in [16]–[24]. DC-side modeling of power electronic systems as impedance is reported in [16]–[18] for dc applications. These works show that the small-signal analysis is a suitable method to linearize the power electronic systems. Furthermore, the impedance stability criteria can be applied to assess the relative stability by means of Nyquist or Bode diagrams [16]–[18]. This is further extended to multiterminal dc systems in [19]. On the other hand, different control techniques for MVDC bus voltage (e.g., linearization via state feedback, backstepping, linear quadratic Gaussian, and synergetic control), in systems with buck converters connected to CPLs, are proposed and compared in [20]–[24]. Most of the literature focuses on the CPL behavior of the load side, whereas a comparison of active and passive rectifiers, when supplying pulsed loads, is given in [25]. This comparison encompasses performance aspects like the response time to the changes in the pulsed load and the voltage control of the dc-side.

This paper analyzes a possible MVDC electrical distribution system for a large marine vessel with power levels of several megawatts (MWs), considering the proven and available industrial technologies. Small-signal modeling and linear analysis at selected operation points is performed in order to identify the potential unstable conditions that may compromise the MVDC system design [1], [17], [18]. In order to analyze the source–load dynamic interactions, reasonable simplifications are made to the complex system. The dynamic assessment includes the contribution of the generator inductances, dc-bus capacitors, cable effects, and source and load control strategies, which includes the modeling of the CPL behavior. Nyquist plots are shown as design figures of merit that provide insightful information about the key aspects that the design of the future MVDC electrical distribution systems can consider.

This paper is organized as follows. The MVDC electrical distribution system is discussed in Section II, followed by the

Manuscript received September 20, 2016; revised December 7, 2016; accepted January 5, 2017. Date of publication February 23, 2017; date of current version May 10, 2017.

U. Javaid, F. D. Freijedo, and D. Dujic are with the Power Electronics Laboratory, École Polytechnique Fédérale de Lausanne, CH-1015 Lausanne, Switzerland (e-mail: uzair.javaid@epfl.ch; francisco.freijedo@epfl.ch; drazen.dujic@epfl.ch).

W. van der Merwe is with the Department of Medium Voltage Drives, ABB Switzerland Ltd., CH-5300 Turgi, Switzerland (e-mail: wim.van-der-merwe@ch.abb.com).

Color versions of one or more of the figures in this paper are available online at http://ieeexplore.ieee.org.

Digital Object Identifier 10.1109/TIE.2017.2674597

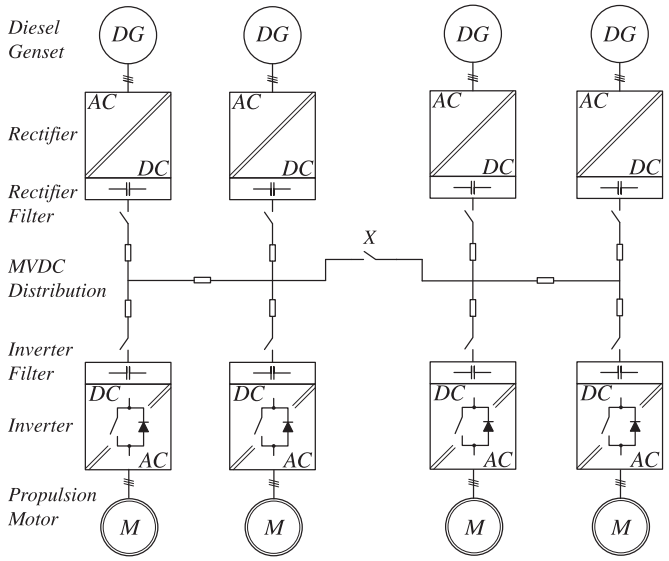

Fig. 1. Ship on-board MVDC electrical distribution system.

description of the impedance-based stability criteria and assumptions for the system linearization in Section III. Determination of the impedance/admittance of the source/load subsystems is discussed in Section IV, followed by the dynamic stability analysis in Section V. Section VI provides the summary and conclusions of this paper.

II. System Description—MVDC Electrical Distribution

The marine electrical distribution systems are isolated grids, with short distribution distances and special challenges arising from the power levels that depend on the functionality of the vessel [26]. These systems are going through rapid changes due to the advancements in the power electronic technologies, and an aggregation of these changes provides an opportunity to gradually phase out the existing MVAC distribution with the MVDC distribution. A possible, albeit simplified, architecture of an MVDC electrical distribution system for a large marine vessel, with several tens of MW power levels, is illustrated in Fig. 1. The system consists of four diesel generators connected to rectifiers with each one having its own filter and disconnector connecting them to the MVDC distribution. These distribution systems are normally expected to be redundant and can be interconnected through the switch X in the case of loss of generation on either side. Each side of the MVDC distribution is supplying two propulsion drives having inverter filters, inverters, and motors. As propulsion loads make up nearly 80% of the load [26], the auxiliary smaller loads such as hotel loads, pumps, and direct-to-line motors are omitted from considerations. All parts of the system are briefly described below.

A. Diesel Generator Sets

The diesel generator sets are the power house of the ship on-board electrical power systems [27] and are represented with DG in Fig. 1. Gas turbines can also be employed as the main power generators when coupled with high-speed generators for military vessels, with power levels up to 40 MW [28], but they are not considered for this study. The diesel generator sets are usually combination of two discrete parts: 1) prime mover, which is usually a medium-to-high-speed diesel engine providing input mechanical power; and 2) 3ϕ synchronous generator, which produces the electrical power. These generators are also medium to high speed with two to ten poles, with a frequency of or 60 Hz and voltage levels of or 6.6 kV, with their excitation being controlled by an automatic voltage regulator (AVR) [14], [26]. As no transformers are being used for the voltage coordination in this study and the prospective MVDC system, the voltage of the generators and the distribution system is identical to the voltage class of the propulsion motors.

B. Rectifiers

Rectifiers play a pivotal role as they connect the MVAC power generation to the MVDC distribution by converting the ac voltage to the dc voltage. In the existing MVAC distribution, propulsion drives have their own rectifiers, e.g., a 12-pulse rectifier is reported in [29]. Some literature works considering multiples of 3ϕ generators can be found leading to the utilization of multiples of six-pulse rectifiers [30]–[32], but most of the MVAC distribution in ships is based on 3ϕ systems [26]. Therefore, in this case, 3ϕ generators with six-pulse rectifiers, which can either be diode rectifiers, thyristor rectifiers, or active rectifiers, are considered. Taking into account the present voltage-blocking capabilities of semiconductors, realization of MVDC rectifiers would require series connection of several devices depending on the distribution voltage level [33], increasing the overall design complexity.

C. Filters

In the existing back-to-back propulsion drives, a central dc-link capacitance is used, which decouples the rectifier from the inverter. In our case, where the rectifier and inverter sides are connected through distribution cables, a possible scenario for this filtering effort is to be shared between the rectifier filter and the inverter filter. The new arrangement of the dc-link capacitors is shown in Fig. 1. Different filters are required depending on the topology of the rectifier, e.g., in our case, six-pulse thyristor rectifier has LC filters, while for diode rectifier and active rectifiers, only capacitive filters are used [34].

D. Cables

To distribute electrical energy throughout the ship and connect the rectifiers and the inverters, a cable-based MVDC distribution system, in bipolar configuration, has been considered. It should be noted that commercial cables are designed for MVAC applications [14], [36], so there is a need to develop the MVDC cables. Nonetheless, a single-pole 12-kV XPLE MVAC cable is being considered in the paper [36]. The distances between sources and loads, in marine electrical distribution systems, are typically from few tens of meters to a few hundred meters (up to 1 km are considered for this study). The cables introduce

TABLE I
SYSTEM PARAMETERS USED FOR THIS STUDY

System Parameters	
Rated Apparent Power S_n	7 MVA
Rated Direct Voltage $V_{\mathrm{dc}.n}$	5 kV
Rated Frequency f_g	50 Hz
Phase Reactor Inductance	$0.1\frac{V_{\mathrm{dc},n}^2}{2\pi f_g S_n}$
Phase Reactor Resistance	3 mΩ
Switching Frequency	250 Hz
Induction Motor Ratings	
Rated Power	6.5 MW
Rated Voltage	3.05 kV
Rated Current	1.4 kA
Rated Frequency	19 Hz
Rated Speed	376 r/min
Power Factor	0.92
Cable Parameters	
Line Inductance	0.347 mH·km^{-1}
Line Resistance	0.089 Ω·km^{-1}
Line Capacitance	0.307 μF·km^{-1}

additional inductances and capacitances in the system that can lead to resonances located either in the low- or high-frequency spectrum, depending on the length. Different models have been proposed for ac cables to simulate them with good accuracy [37]. One aspect that sets ac and dc cables aside is the lack of skin effect in dc cables; therefore, a simplified version of these ac cable models can be used for dc cable studies. These models can have different degrees of complexity depending on the level of the required accuracy, but most of them are not suited for small-signal analysis. The π-section model is simplest among them and will be used for this study. It is fairly accurate for this study with short cable lengths and considering use of high-power medium-voltage semiconductors, characterized with rather modest switching frequencies (few hundreds of hertz; more details are in the next subsection) but also not high dv/dt, a single π-section can represent a frequency up to 37.5 kHz for a cable length of 1 km. This can be calculated by $f_{\max} = N\nu/8l_{\mathrm{tot}}$, where $f_{\max}$ is the maximum frequency that can be represented by π-sections, N is the number of π-sections required, ν is the speed of propagation of the wave, and l_{tot} is the total length of the cable [37]. The cable parameters are given in Table I.

E. Inverters

Different drive technologies exist for industrial and ship applications. The converter topologies employed are usually multilevel voltage-source inverters [38]. Vector controls of motors, e.g., field-oriented control (FOC) and direct torque control, are used as the control of the propulsion drives [32]. Here, FOC is considered for the propulsion drives. In high-power drives, to minimize the switching losses, lower switching frequencies are used. This switching frequency can be as low as 150 Hz for integrated-gate commutated-thyristor (IGCT)-based high-power drives, mostly limited by thermal constraints [39]. The switching frequency in this work is selected as 250 Hz [32].

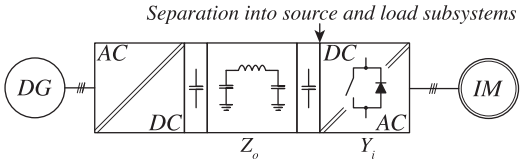

Fig. 2. Two-port MVDC distribution system. The system is partitioned at the arrow in accordance with stability definition and the conditions for measuring impedance/admittance [16], [35].

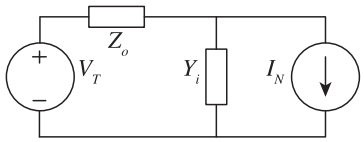

Fig. 3. Linearized equivalent model of a two-port MVDC system for stability analysis.

F. Propulsion Motors

Propulsion motors make up almost 80% of the load of the ship power system, converting the electrical power to mechanical work. They are predominately induction motors because of their rugged design and less maintenance. Synchronous motors are mostly used where power levels exceed 5 MW [26]. With the popularity and availability of permanent magnet synchronous motors, they are being increasingly considered for high-power application, e.g., podded propulsion uses these motors. For the sake of generality, induction motors are considered as propulsion motors for this study.

III. SYSTEM DYNAMIC ASSESSMENT BASED ON IMPEDANCE STABILITY CRITERIA

As explained earlier, the scope of this paper is to quantify the effect of the generator and filter inductances, the filter capacitors, the source-side converter control strategy, and the cable inductances on the possible resonances in the system and their implications on stability. Fig. 1 represents a complex system. Using basic linear properties (e.g., superposition principle), a complex system like in Fig. 1 can be scaled down to a simplified circuit like in Fig. 2 [17], [18], by assuming that both the sources and the loads are working with similar loading cycles, respectively. A key feature of Fig. 2 is that it shows equivalent source and load. For the sake of generality, this simplified two-port system is suitable to extract figures of merit for each different source and load devices. Physically, the system of Fig. 2 can also be divided into different subsystems, i.e., generator, rectifier, filter at the source, distribution cable (represented as an equivalent π-section model), input capacitor, and inverter as a load. For impedance stability analysis, Fig. 2 should be further simplified to Fig. 3 [16], [18], [35]. Therefore, the physical components are grouped in a source or load side accordingly. Fig. 2 shows the partition point considered for the analysis. Overall, the source side is modeled as a Thevenin equivalent because it is supporting the voltage. On the other hand, the load side is injecting current into the motor; therefore, it can be modeled as a Norton equivalent. It should be noted that the Norton equivalent

TABLE II
SYSTEM PARAMETERS AND THEIR VARIATIONS TO EMULATE DIFFERENT CONDITIONS

Parameter	Value
Generator Frequency	50–100 Hz
System Load	25–100%
Rectifier Filter	1–10 mF
Cable Length	10 m–1 km
Inverter Filter	1–10 mF

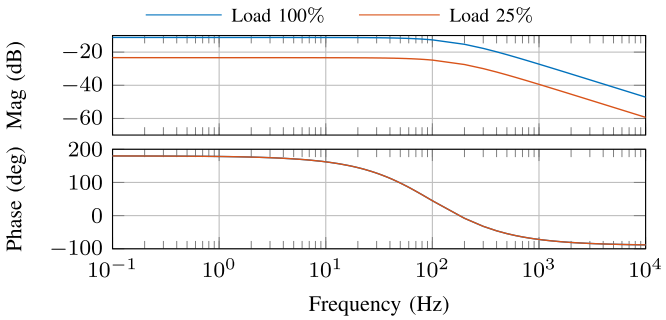

Fig. 4. Load admittance in a frequency window of 0.1 Hz to 10 kHz.

captures the CPL behavior of inverter drives. The source voltage V_T, the load current I_N, the output impedance of the source Z_o, and the input load admittance Y_i must all be stable. The product $Z_o(j\omega)Y_i(j\omega)$ is employed to construct the Nyquist contours to assess the stability of the system under consideration.

IV. IMPEDANCE AND ADMITTANCE MEASUREMENT OF THE SOURCE AND LOAD SUBSYSTEMS

The dynamic assessment of the system, given in Fig. 2, is carried out for three different source-side converters, e.g., diode rectifier, thyristor rectifier, and active rectifier with variations in the generator frequencies, filter sizes, distribution cable lengths, and the loading conditions. These variations in the system parameters are listed in Table II. For the impedance/admittance measurement of the source/load subsystem, the current/voltage perturbations, as a multitone signal, are applied at the terminals, and corresponding voltage/current is measured. The ratio of the measured signal due to the applied perturbations gives us the impedance/admittance of the subsystem. The frequency window used is from 0.1 Hz to 10 kHz, as it is sufficient to capture all the expected resonances.

A. Load Admittance—Propulsion Drive

The load side considers an induction motor drive that is controlled with FOC. The parameters of the induction motor are given in Table I. Load admittance, shown in Fig. 4, is measured for full load, i.e., 100% of the rated speed and rated torque, and light load, i.e., 100% of the rated speed and 25% rated torque. The admittances show negative resistance characteristics for a majority of the frequency window but changes to an inductive behavior later on due to the limitations on the current control bandwidth, imposed by the switching frequency of the medium-voltage inverter. Therefore, the motor inductances dominate the load admittance at higher frequencies.

TABLE III
CIRCUIT PARAMETERS VARIATION DUE TO PARAMETRIC SWEEP OF TABLE II

Line Inductance $2L_{\text{line}}$	
6.94 μH @10 m	0.694 mH @1 km
Phase Reactor Inductance L_g	
1.137 mH @50 Hz	0.568 mH @100 Hz
Filter Inductance L (Valid only for Thyristor rectifier)	
1.53 mH @50 Hz, $C_{\text{rec}} = 1$ mF	0.115 mH @50 Hz, $C_{\text{rec}} = 10$ mF
0.25 mH @100 Hz, $C_{\text{rec}} = 1$ mF	0.044 mH @100 Hz, $C_{\text{rec}} = 10$ mF

B. Source Impedance—Diode Rectifier

The first case considers the diode rectifier. The schematics is given in Fig. 5(a). To maintain the dc-link voltage, the AVR of the generator is used. The feedback to the AVR comes from the rectifier filter dc-link voltage. The AVR is based on a simple P controller. To filter the output voltage of the diode rectifier, a capacitive filter C_{rec} is used. Impedances for the diode rectifier, shown in Fig. 6(a), are measured considering the parametric variations listed in Table II. All the resonances in the source impedance are caused by the inductances and capacitances in the circuit. The first resonance, in Fig. 6(a) and shaded blue, is because of the generator inductance and the filter capacitors. The line inductance is smaller and only acts at higher frequencies, so it does not play any part here. The natural resonance frequency can be calculated by

$$f_{\text{LC}} = \frac{1}{2\pi\sqrt{2L_g C_1}}. \tag{1}$$

Here, $C_1 = C_{\text{rec}} + C_{\text{inv}}$. Note that the value of C_{line} is very small compared to the C_{rec} or C_{inv}; therefore, it is neglected here. Fig. 1 is only valid for $L_g \gg L_{\text{line}}$, but if $L_g \approx L_{\text{line}}$, then the approximation of the line inductance acting higher frequencies is no longer valid and the resonance frequency is not that straightforward to determine. The second natural resonance, shaded red in Fig. 6(a), occurs at higher frequency, due to the line inductances and the rectifier and inverter capacitances, while the much higher generator inductance can be considered as open circuit for this. It can be calculated as

$$f_{\text{CLC}} = \frac{1}{2\pi}\sqrt{\frac{1}{L_{\text{line}}}\left(\frac{1}{C_{\text{rec}}} + \frac{1}{C_{\text{line}}}\right)}. \tag{2}$$

Since L_g varies with the changes in generator frequency and so does the frequency at which the first resonance occurs. It can also be seen that if the distribution cable length is longer, the resonance occurs at lower frequencies due to higher line inductance and occurs at higher frequencies for shorter lengths due to smaller line inductance. These changes in L_g and line inductance and their effect are illustrated in Fig. 6(a) and Table III. The natural resonance frequencies are given in Table IV for the diode rectifier case and system configurations considered in this paper.

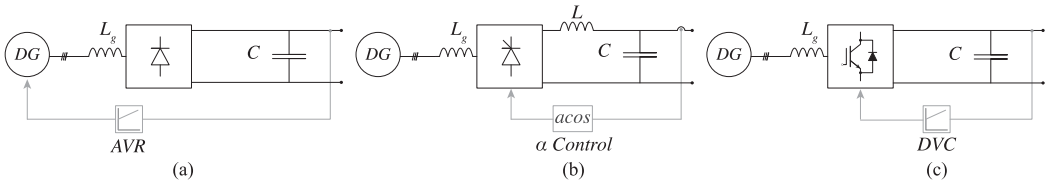

Fig. 5. Different source-side converters. (a) Diode rectifier. (b) Thyristor rectifier. (c) Active rectifier.

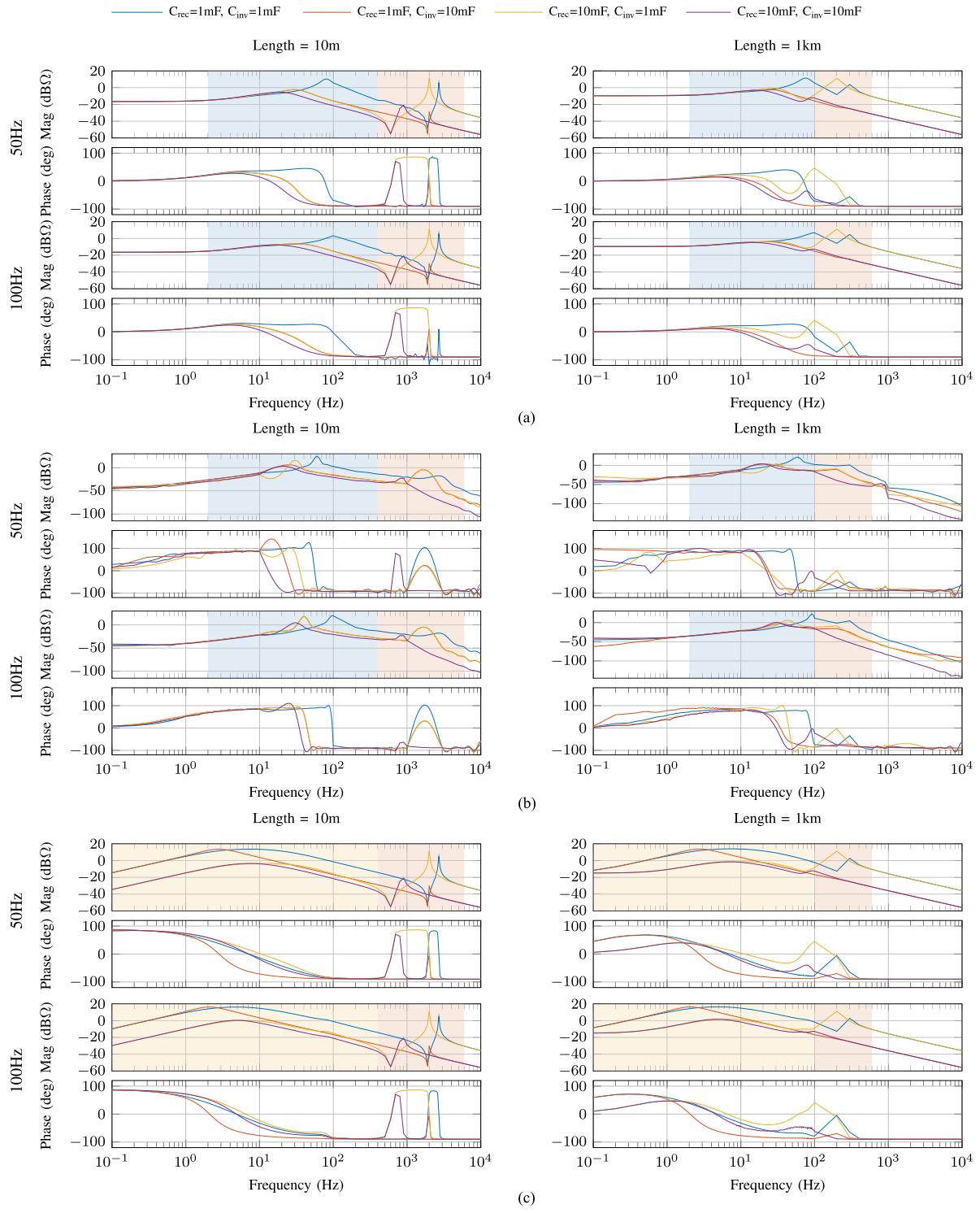

Fig. 6. Source impedances in a frequency window of 0.1 Hz to 10 kHz for different filtering efforts. (a) Diode rectifier. (b) Thyristor rectifier. (c) Active rectifier.

TABLE IV
NATURAL RESONANCE FREQUENCIES FOR A DIODE RECTIFIER USING (1) AND (2)

System Configurations	f_{LC}	f_{LCL}
$f_g = 50$ Hz		
$C_{\mathrm{rec}} = 1$ mF, $C_{\mathrm{inv}} = 1$ mF, 10 m	75 Hz	2701 Hz
$C_{\mathrm{rec}} = 1$ mF, $C_{\mathrm{inv}} = 10$ mF, 10 m	32 Hz	2003 Hz
$C_{\mathrm{rec}} = 10$ mF, $C_{\mathrm{inv}} = 1$ mF, 10 m	32 Hz	2003 Hz
$C_{\mathrm{rec}} = 10$ mF, $C_{\mathrm{inv}} = 10$ mF, 10 m	24 Hz	854.5 Hz
$C_{\mathrm{rec}} = 1$ mF, $C_{\mathrm{inv}} = 1$ mF, 1 km	75 Hz	270.1 Hz
$C_{\mathrm{rec}} = 1$ mF, $C_{\mathrm{inv}} = 10$ mF, 1 km	32 Hz	200.3 Hz
$C_{\mathrm{rec}} = 10$ mF, $C_{\mathrm{inv}} = 1$ mF, 1 km	32 Hz	200.3 Hz
$C_{\mathrm{rec}} = 10$ mF, $C_{\mathrm{inv}} = 10$ mF, 1 km	24 Hz	85.4 Hz
$f_g = 100$ Hz		
$C_{\mathrm{rec}} = 1$ mF, $C_{\mathrm{inv}} = 1$ mF, 10 m	106 Hz	2701 Hz
$C_{\mathrm{rec}} = 1$ mF, $C_{\mathrm{inv}} = 10$ mF, 10 m	45 Hz	2003 Hz
$C_{\mathrm{rec}} = 10$ mF, $C_{\mathrm{inv}} = 1$ mF, 10 m	45 Hz	2003 Hz
$C_{\mathrm{rec}} = 10$ mF, $C_{\mathrm{inv}} = 10$ mF, 10 m	34 Hz	854.5 Hz
$C_{\mathrm{rec}} = 1$ mF, $C_{\mathrm{inv}} = 1$ mF, 1 km	106 Hz	270.1 Hz
$C_{\mathrm{rec}} = 1$ mF, $C_{\mathrm{inv}} = 10$ mF, 1 km	45 Hz	200.3 Hz
$C_{\mathrm{rec}} = 10$ mF, $C_{\mathrm{inv}} = 1$ mF, 1 km	45 Hz	200.3 Hz
$C_{\mathrm{rec}} = 10$ mF, $C_{\mathrm{inv}} = 10$ mF, 1 km	34 Hz	85.4 Hz

C. Source Impedance—Thyristor Rectifier

A thyristor rectifier is considered for the second case with the schematics given in Fig. 5(b). This configuration can control the voltage of the dc-link within a certain voltage band. To maintain the dc-link voltage, a modified inverse cosine control is used with dc-side current as feedback [34]. This helps in correcting the thyristor firing angle α to an appropriate value. The output of this configuration requires an LC filter. As the impedances, shown in Fig. 6(b), are measured considering the parametric variations listed in Table II, any changes in the value of the filter capacitor, in the LC filter, lead to changes in the inductance as well. This inductance can be calculated for a constant cutoff frequency and is given by

$$L = \frac{V_{\mathrm{ripple}}}{12\pi f_g I_{\mathrm{DCmin}}}. \tag{3}$$

Here, V_{ripple} is the ripple voltage and I_{DCmin} is the minimum current dc current (10% of the rated current) in the load. Different values of L are given in Table III.

The controllability of the thyristor rectifier is visible only in the lower frequency range up to 2 Hz, whereas all the resonances, in source impedance plots of Fig. 6(b), are caused by the inductances and capacitances in the circuit. The first resonance also has the effect of the filter inductance; therefore, (1) is modified and the new expression is given as follows:

$$f_{\mathrm{LC}} = \frac{1}{2\pi\sqrt{L_1 C_1}}. \tag{4}$$

Here, $L_1 = 2L_g + L$ and $C_1 = C_{\mathrm{rec}} + C_{\mathrm{inv}}$. The second resonance occurs at higher frequencies and is because of the line inductances and the rectifier and inverter capacitances and is determined using (2).

TABLE V
SUMMARY OF THE ASSESSMENT OF THE DIFFERENT SOURCE-SIDE CONVERTERS FOR $f_g = 50$ Hz AND 100 Hz AT 100% LOADING

	$\eta_1 \geq 0.5$ (stable)	$0.5 > \eta_1 > 0.1$ (weakly stable)	$\eta_1 \leq 0.1$ (unstable)
Cable length 10 m, $C_{\mathrm{rec}} = 1$ mF			
$C_{\mathrm{inv}} = 1$ mF	A	B	C
$C_{\mathrm{inv}} = 10$ mF	A, B	–	C
Cable length 10 m, $C_{\mathrm{rec}} = 10$ mF			
$C_{\mathrm{inv}} = 1$ mF	A, B, C	–	–
$C_{\mathrm{inv}} = 10$ mF	A, B, C	–	–
Cable length 1 km, $C_{\mathrm{rec}} = 1$ mF			
$C_{\mathrm{inv}} = 1$ mF	A	B	C
$C_{\mathrm{inv}} = 10$ mF	A, B	–	C
Cable length 1 km, $C_{\mathrm{rec}} = 10$ mF			
$C_{\mathrm{inv}} = 1$ mF	A, B, C	–	–
$C_{\mathrm{inv}} = 10$ mF	A, B, C	–	–

D. Source Impedance—Active Rectifier

The third case considers an active rectifier. The schematics of this arrangement is given in Fig. 5(c). The active rectifier is controlled through the cascaded voltage and current control loops. The voltage control is based on direct voltage control, and detailed description of this control is given in [40]. Only a capacitive filter is used in this case. Source impedance for the active rectifier case is given in Fig. 6(c). The impedances that are shown in Fig. 6(c) can be determined mathematically by simplification of the control and the cable π-model. The control has an outer voltage control loop and an inner current control loop. The current control is considered to have sufficient bandwidth; therefore, its impact on the voltage loop is ignored. The converter impedance can be modeled as

$$Z_{\mathrm{conv}} = \frac{s}{s^2 C_{\mathrm{rec}} + \frac{k_p s}{\sqrt{3}} + \frac{k_i}{\sqrt{3}}}. \tag{5}$$

The π-section model of the line is being considered for this study. From Table I, it can be seen that the capacitances are very small and can be neglected in these theoretical considerations. Thus, the line can be represented just as an RL circuit, as

$$Z_{\mathrm{line}} = sL_{\mathrm{line}} + R_{\mathrm{line}}. \tag{6}$$

The impedance of capacitor bank on the inductor side can be represented as $Z_{C_{\mathrm{inv}}} = 1/sC_{\mathrm{inv}}$. Adding all these impedances give us the expression for the total source output impedance. The total source output impedance is given as

$$Z_o = (Z_{\mathrm{conv}} + Z_{\mathrm{line}}) \,||\, Z_{C_{\mathrm{inv}}}. \tag{7}$$

From Fig. 6(c), it can be seen that for the long line, i.e., 1 km case, the higher resistance is also dominant at lower frequencies, i.e., 1 Hz. The first resonance, shaded yellow in Fig. 6(c), is dependent on the controller parameters k_p and k_i and can be calculated as given in [40], while the second resonance is given by (2).

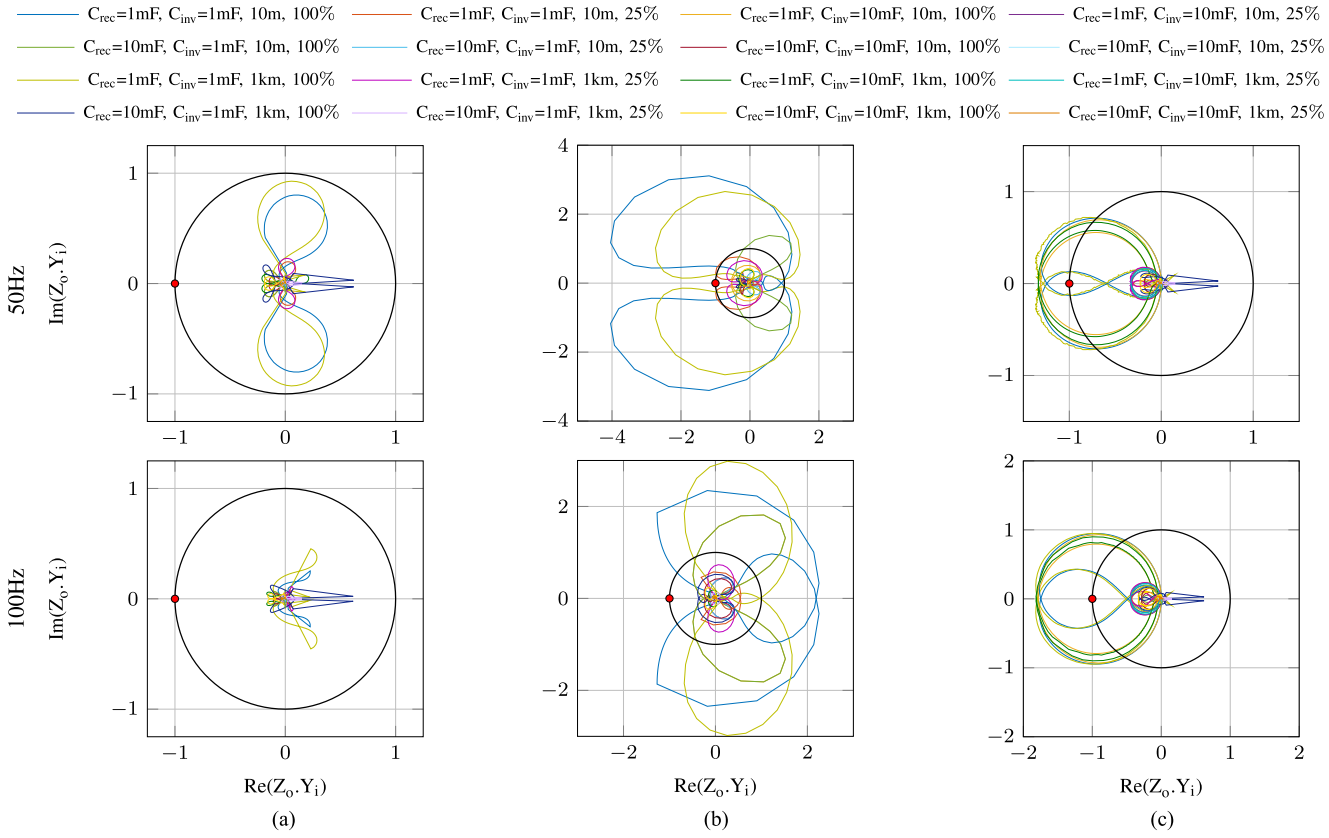

Fig. 7. Nyquist plots for the different system configurations and loadings. (a) Diode rectifier. (b) Thyristor-controlled rectifier. (c) Active rectifier.

V. Small-Signal Stability Assessment

The stability of the equivalent two-port MVDC system is evaluated for the different system configurations of Table II. These parameters point toward possible system configurations that could be found in the future MVDC systems [14]. For the system to exhibit absolute stability, it must satisfy the Nyquist stability criterion, i.e., it must not encircle $(-1, 0)$. Furthermore, a relative stability metric should be employed, as required in the IEEE Std. 1709-2010 [1]. The inverse of the sensitivity peak η_1 is used here, as it is especially suited for system with resonances [41]. This factor can help categorize the system as an $\eta_1 > 0.5$ illustrates high stability margin, $0.5 < \eta_1 > 0.1$ exhibits low stability margins, and $\eta_1 < 0.1$ points toward unstable behavior [41], [42]. The observations from Nyquist plots, which are discussed below, are summarized in Table V, with A, B, and C representing the diode rectifier, the thyristor rectifier, and the active rectifier, respectively.

The Nyquist trajectories for the different source configurations and the two different loading conditions at $f_g = 50$ Hz and $f_g = 100$ Hz are given in Fig. 7. Fig. 7(a) shows the Nyquist plots for the diode rectifier case, where the upper plot is for $f_g = 50$ Hz and the bottom plot for $f_g = 100$ Hz. It can be seen that none of the Nyquist trajectories for the different system configurations intersect the unit circle or encircle the critical point of $(-1, 0)$. In the upper plot of Fig. 7(a), two system configurations, with $f_g = 50$ Hz, $C_{\text{rec}} = C_{\text{inv}} = 1$ mF, and cable lengths 10 m and 1 km, have trajectories close to the unit circle that do not intersect it, which means that the absolute stability criterion is fulfilled in all the cases. Moreover, all of the cases fulfill the relative stability criterion $\eta_1 > 0.5$. The time-domain simulation of a representative case is shown in Fig. 8(a).

Nyquist trajectories for the thyristor rectifier case are shown in Fig. 7(b). As discussed in the earlier section, the inductance of the filter (on the dc-side) plays a key role in the resonance of the system, e.g., its value from the design is especially high for the combination of the lower frequency of the generator and the low filter capacitance, as can be observed from Table III. As shown in Fig. 7(b), three system configurations with $f_g = 50$ Hz intersect the unit circle. Even though they do not encircle the critical point of $(-1, 0)$, two of them ($C_{\text{rec}} = C_{\text{inv}} = 1$ mF and cable lengths 10 m and 1 km, with both high and low loading) intersect the unit circle close to the critical point. The relative stability index, for these system configurations, is in the range of $0.5 < \eta_1 > 0.1$, which means that these configurations have a weakly stable behavior at 100% loading. This behavior may represent underdamped or self-sustained oscillations. The other system configuration that intersects the unit circle is $C_{\text{rec}} = 10$ mF, $C_{\text{inv}} = 1$ mF, and cable length of 10 m, but has a high relative stability margin (i.e., $\eta_1 > 0.5$). For the case of $f_g = 100$ Hz, the configurations discussed above again intersect the unit circle, but all have high relative stability margin, i.e., $\eta_1 > 0.5$. Any possible instabilities, in this system, might come from the increase in the system inductance due to the presence of the LC filter at the output of the thyristor rectifier. The time-

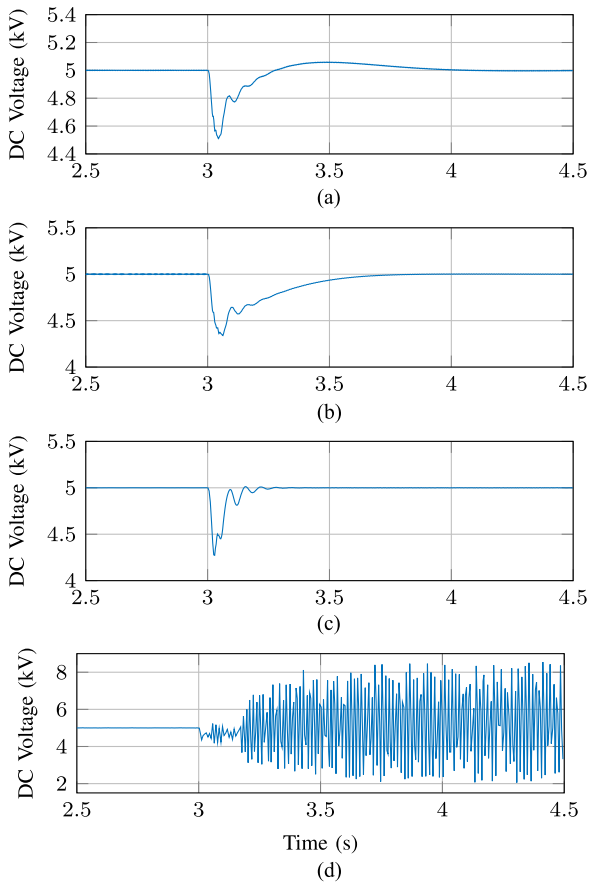

Fig. 8. Time-domain simulations showing the dc-side voltage for the different source converters, when a step change from 0.25% to 100% load is applied at 3 s. (a) Diode rectifier for 50 Hz, $C_{\text{rec}} = C_{\text{inv}}$ = 1 mF, 10 m. (b) Thyristor-controlled rectifier for 50 Hz, $C_{\text{rec}} = C_{\text{inv}} =$ 1 mF, 10 m. (c) Active rectifier for the stable case: 50 Hz, $C_{\text{rec}} =$ 10 mF, $C_{\text{inv}} =$ 1 mF, 10 m. (d) Active rectifier for unstable case: 100 Hz, $C_{\text{rec}} = C_{\text{inv}} =$ 1 mF, 1 km. Note: The bandwidths of the AVR for a diode rectifier and a voltage controller for a thyristor-controlled rectifier are the same. (a) Diode rectifier. (b) Thyristor-controlled rectifier. (c) Active rectifier—stable case. (d) Active rectifier—unstable case.

domain simulation of a representative case is given in Fig. 8(b), which shows that the system is stable and the oscillations are well damped.

The discussion on the source impedance of the active rectifier shows that the lower frequency resonance is dependent on the control, and the higher frequency resonance is dependent on the parameters of the circuit. As shown in Fig. 7(c), four configurations ($C_{\text{rec}} = 1$ mF, $C_{\text{inv}} = 1$ mF, 10 mF, and cable length 10 m, 1 km) of the system are showing unstable behavior as they encircle the critical point of $(-1, 0)$. These instabilities are due to the low value of the source-side capacitance, which decreases the controller's ability to damp the oscillations due to L_g. All the other configurations show high relative stability of $\eta_1 < 0.1$, thus showing the oscillation damping capability of the voltage controller. Same configurations also exhibit unstable behavior for $f_g = 100$ Hz. The time-domain simulations of representative cases, stable and unstable, are given in Fig. 8(c) and (d), respectively. Both time-domain simulations verify the predictions of the Nyquist plots and are summarized in Table V. From Fig. 8(c), it can be seen that the active rectifier, with proper filtering effort, exhibits well-damped response to the load change.

From these results, it can be seen that the diode rectifier exhibits the best dynamic behavior of the three source converters for the system and operating conditions. Practically, the diode rectifier is simple, robust, and inexpensive, but it is dependent on AVRs of the generators that are slow and have a low bandwidth for any changes in the output voltage. The thyristor-controlled rectifier has its dynamics slightly penalized by its large inductive filter on the dc-side and exhibits potentials for resonances in the system. But the advantage of thyristor-controlled rectifier is its ability to control the dc-side voltage itself, but also suffers from low bandwidth, the inability to step up the voltage, and is expensive. An active rectifier, on the other hand, with a proper dc-side capacitance can maintain the dc-side voltage under all loading conditions and has a high bandwidth that contributes highly to the stability of the system. Additionally, active rectifier also allows for bidirectional power flow, but it adds (practical) complexity and cost to the system.

VI. Conclusion

This paper focused on the dynamics associated with load/source interactions in marine MVDC power systems. The analysis presented in the paper has been restricted to the available industrial products that are likely to be deployed by the early adopters of the MVDC systems. For that reason, the considered source-side converters are diode-, thyristor-, and active-rectifiers, supplying the vector-controlled propulsion drives, which are normally the largest loads in a system. Therefore, a dynamic assessment of the source–load interactions, considering contributions from generator inductances, dc-bus side capacitances, impact of cables, and the control strategies of source and load sides (constant power load behavior), provides valuable insights about expected interactions in marine on-board MVDC power distribution. To extract the proper figures of merit, impedance stability analysis is used and the Nyquist trajectories are plotted and analyzed for the dynamic assessment giving valuable insights. It has been proven that the increase in the source-side system inductance and the decrease in the capacitive filtering can lead to an unstable behavior, which is highlighted in the thyristor-controlled rectifier and active rectifier cases. The diode rectifier is simple and inexpensive, but cannot control the dc-side voltage that is in turn controlled by the AVR control of the generator. The thyristor-controlled rectifier provides controllability of the dc-side voltage with a low bandwidth controller, but can only step-down the voltage. Finally, the active rectifier offers a better dynamic response near rated conditions, but is sensitive to changes in filtering effort, cables, and interaction between load and source leading to unstable behavior and also is more complex and expensive.

Both diode- and active-rectifiers are part of the state-of-the-art VSI-based back-to-back drives, therefore, may be preferred over thyristor-controlled rectifier. The decision to utilize either of them will highly depend on additional factors, such as the presence of on-board energy storage (bidirectional power flow), requirement of high bandwidth dynamics of the source, cost, and reliability.

REFERENCES

[1] *IEEE Recommended Practice for 1 kV to 35 kV Medium-Voltage DC Power Systems on Ships*, IEEE Standard 1709, 2010.

[2] T. J. McCoy, "Trends in ship electric propulsion," in *Proc. Power Eng. Soc. Summer Meeting*, Jul. 2002, vol. 1, pp. 343–346.

[3] J. Amy, Jr, "Modem, high-converter-populations argue for changing how to design naval electric power systems," in *Proc. IEEE Electr. Ship Technol. Symp.*, 2005, pp. 280–283.

[4] N. H. Doerry and H. Fireman, "Designing all electric ships," in *Proc. 9th Int. Marine Design Conf.*, 2006, pp. 475–498.

[5] N. Doerry and K. McCoy, "Next generation integrated power system: NGIPS technology development roadmap," Naval Sea Syst. Command, Washington, DC, USA, Tech. Rep. ADA519753, 2007.

[6] A. Monti, M. Colciago, P. Conti, M. Maglio, and R. A. Dougal, "Integrated simulation of communication, protection, and power in MVDC systems," in *Proc. IEEE Elect. Ship Technol. Symp.*, Apr. 2009, pp. 353–359.

[7] S. R. Rudraraju, A. K. Srivastava, S. C. Srivastava, and N. N. Schulz, "Small signal stability analysis of a shipboard MVDC power system," in *Proc. IEEE Elect. Ship Technol. Symp.*, Apr. 2009, pp. 135–141.

[8] B. Zahedi and L. E. Norum, "Efficiency analysis of shipboard dc power systems," in *Proc. 39th Annu. Conf. IEEE Ind. Electron. Soc.*, Nov. 2013, pp. 689–694.

[9] M. Cupelli, M. Moghimi, A. Riccobono, and A. Monti, "A comparison between synergetic control and feedback linearization for stabilizing MVDC microgrids with constant power load," in *Proc. IEEE PES Innovative Smart Grid Technol., Eur.*, Oct. 2014, pp. 1–6.

[10] J. Shi, R. Amgai, and S. Abdelwahed, "Modelling of shipboard medium-voltage direct current system for system level dynamic analysis," *IET Elect. Syst. Transp.*, vol. 5, no. 4, pp. 156–165, 2015.

[11] M. Cupelli *et al.*, "Power flow control and network stability in an all-electric ship," *Proc. IEEE*, vol. 103, no. 12, pp. 2355–2380, Dec. 2015.

[12] H. Holttinen *et al.*, "Currents of change," *IEEE Power Energy Mag.*, vol. 9, no. 6, pp. 47–59, Nov. 2011.

[13] A. Tessarolo, S. Castellan, R. Menis, and G. Sulligoi, "Electric generation technologies for all-electric ships with medium-voltage dc power distribution systems," in *Proc. IEEE Elect. Ship Technol. Symp.*, Apr. 2013, pp. 275–281.

[14] U. Javaid, D. Dujic, and W. van der Merwe, "MVDC marine electrical distribution: Are we ready?" in *Proc. 41st Annu. Conf. IEEE Ind. Electron. Soc.*, Nov. 2015, pp. 823–828.

[15] A. Emadi, A. Khaligh, C. H. Rivetta, and G. A. Williamson, "Constant power loads and negative impedance instability in automotive systems: Definition, modeling, stability, and control of power electronic converters and motor drives," *IEEE Trans. Veh. Technol.*, vol. 55, no. 4, pp. 1112–1125, Jul. 2006.

[16] P. Liutanakul, A. B. Awan, S. Pierfederici, B. Nahid-Mobarakeh, and F. Meibody-Tabar, "Linear stabilization of a dc bus supplying a constant power load: A general design approach," *IEEE Trans. Power Electron.*, vol. 25, no. 2, pp. 475–488, Feb. 2010.

[17] A. Riccobono and E. Santi, "Comprehensive review of stability criteria for dc power distribution systems," *IEEE Trans. Ind. Appl.*, vol. 50, no. 5, pp. 3525–3535, Sep./Oct. 2014.

[18] S. D. Sudhoff, S. F. Glover, P. T. Lamm, D. H. Schmucker, and D. E. Delisle, "Admittance space stability analysis of power electronic systems," *IEEE Trans. Aerosp. Electron. Syst.*, vol. 36, no. 3, pp. 965–973, Jul. 2000.

[19] J. Sun, "Autonomous local control and stability analysis of multiterminal dc systems," *IEEE Trans. Emerg. Sel. Topics Power Electron.*, vol. 3, no. 4, pp. 1078–1089, Dec. 2015.

[20] G. Sulligoi, D. Bosich, L. Zhu, M. Cupelli, and A. Monti, "Linearizing control of shipboard multi-machine mvdc power systems feeding constant power loads," in *Proc. IEEE Energy Convers. Congr. Expo.*, Sep. 2012, pp. 691–697.

[21] G. Sulligoi, D. Bosich, G. Giadrossi, L. Zhu, M. Cupelli, and A. Monti, "Multiconverter medium voltage dc power systems on ships: Constant-power loads instability solution using linearization via state feedback control," *IEEE Trans. Smart Grid*, vol. 5, no. 5, pp. 2543–2552, Sep. 2014.

[22] M. Cupelli, M. Mirz, and A. Monti, "Application of backstepping to MVDC ship power systems with constant power loads," in *Proc. Int. Conf. Elect. Syst. Aircraft, Railway, Ship Propulsion Road Vehicles (ESARS)*, Mar. 2015, pp. 1–6.

[23] M. Cupelli, M. Mirz, and A. Monti, "A comparison of backstepping and lqg control for stabilizing MVDC microgrids with constant power loads," in *Proc. IEEE Eindhoven PowerTech*, Jun. 2015, pp. 1–6.

[24] M. Cupelli, A. Monti, E. D. Din, and G. Sulligoi, "Case study of voltage control for mvdc microgrids with constant power loads—Comparison between centralized and decentralized control strategies," in *Proc. 18th Mediterranean Electrotech. Conf.*, Apr. 2016, pp. 1–6.

[25] A. Hasanzadeh, C. S. Edrington, D. M. Soto, and G. M. Rivera, "Comparative study of intensive pulse load impact on active and passive rectification system in MVDC ship power generation unit," in *Proc. Int. Elect. Mach. Drives Conf.*, May 2013, pp. 1326–1332.

[26] A. K. Adnanes, "Maritime electrical installations and diesel electric propulsion," ABB, 2003.

[27] D. Radan, A. J. Sorensen, A. K. Adnanes, and T. A. Johansen, "Reducing power load fluctuations on ships using power redistribution control," *Marine Technol.*, vol. 45, no. 3, pp. 162–174, 2008.

[28] S. Z. Vijlee, A. Ouroua, L. N. Domaschk, and J. H. Beno, "Directly-coupled gas turbine permanent magnet generator sets for prime power generation on board electric ships," in *Proc. IEEE Elect. Ship Technol. Symp.*, May 2007, pp. 340–347.

[29] P. K. Steimer and M. D. Manjrekar, "Practical medium voltage converter topologies for high power applications," in *Proc. 36th IEEE IAS Annu. Meeting*, vol. 3, 2001, pp. 1723–1730.

[30] G. Sulligoi, A. Tessarolo, V. Benucci, M. Baret, A. Rebora, and A. Taffone, "Modeling, simulation, and experimental validation of a generation system for medium-voltage dc integrated power systems," *IEEE Trans. Ind. Appl.*, vol. 46, no. 4, pp. 1304–1310, Jul./Aug. 2010.

[31] G. Sulligoi, A. Tessarolo, V. Benucci, A. M. Trapani, M. Baret, and F. Luise, "Design, implementation and testing of a shipboard medium-voltage dc generation system based on a ultra-high speed 12-phase alternator," in *Proc. IEEE Elect. Ship Technol. Symp.*, Apr. 2011, pp. 388–395.

[32] D. Dujic, J. Wahlstroem, J. A. M. Sosa, and D. Fritz, "Modular medium voltage drive for demanding applications," in *Proc. Int. Power Electron. Conf.*, May 2014, pp. 3476–3481.

[33] J. A. Sayago, T. Bruckner, and S. Bernet, "How to select the system voltage of MV drives—A comparison of semiconductor expenses," *IEEE Trans. Ind. Electron.*, vol. 55, no. 9, pp. 3381–3390, Sep. 2008.

[34] N. Mohan and T. M. Undeland, *Power Electronics: Converters, Applications, and Design*. Hoboken, NJ, USA: Wiley, 2007.

[35] R. D. Middlebrook, "Input filter considerations in design and application of switching regulators," in *Proc. IEEE Ind. Appl. Soc. Annu. Meeting*, 1976, pp. 91–107.

[36] *Brugg Cables—Mittelspannungskabel—Mittelspannungskabel (Cu)—XKDT 1-Leiter MS-Polymerkabel 20/12 kV*, Nov. 2011. [Online]. Available: http://www.bruggcables.com/domains/bruggcables_com/data/free_docs/Katal og_MSNS_de.pdf

[37] M. Zubiaga, A. Cárcar, G. Abad, J. A. Barrena, and S. Aurtenetxea, *Evaluation of the Frequency Response of AC Transmission Based Offshore Wind Farms*. Rijeka, Croatia: InTech, 2011.

[38] J. Wahlstroem, D. Dujic, M. A. Luescher, and S. Reist, "High power IGCT based multilevel inverter," in *Proc. Int. Exhib. Conf. Power Electron., Intell. Motion, Renewable Energy Energy Manage.*, May 2014, pp. 1–6.

[39] J. K. Steinke, "Control strategy for a three phase ac traction drive with three-level GTO PWM inverter," in *Proc. 19th Annu. IEEE Power Electron. Spec. Conf.*, Apr. 1988, vol. 1, pp. 431–438.

[40] L. Harnefors, M. Bongiorno, and S. Lundberg, "Input-admittance calculation and shaping for controlled voltage-source converters," *IEEE Trans. Ind. Electron.*, vol. 54, no. 6, pp. 3323–3334, Dec. 2007.

[41] F. de Bosio, L. A. de Souza Ribeiro, F. D. Freijedo, M. Pastorelli, and J. M. Guerrero, "Effect of state feedback coupling and system delays on the transient performance of stand-alone VSI with LC output filter," *IEEE Trans. Ind. Electron.*, vol. 63, no. 8, pp. 4909–4918, Aug. 2016.

[42] K. J. Astrom and T. Hagglund, *PID Controllers: Theory, Design, and Tuning*. Research Triangle Park, NC, USA: Int. Soc. Autom., 1995.

Uzair Javaid (S'14) was born in Lahore, Pakistan, in 1989. He received the B.Sc. degree in electrical engineering from the University of Engineering and Technology, Lahore, in 2010, and the M.Sc. degree in energy management and sustainability from the École Polytechnique Fédérale de Lausanne (EPFL), Lausanne, Switzerland, in 2013.

Since April 2014, he has been a Doctoral Assistant with the Power Electronics Laboratory, EPFL. His research interests include medium-voltage dc distribution systems, power electronic system modeling and design, and electrical machine drives.

Francisco D. Freijedo (M'07–SM'16) received the M.Sc. degree in physics from the University of Santiago de Compostela, Santiago de Compostela, Spain, in 2002, and the Ph.D. degree in electrical engineering from the University of Vigo, Vigo, Spain, in 2009.

From 2005 to 2011, he was a Lecturer with the Department of Electronics Technology, University of Vigo. From 2011 to 2014, he was with Gamesa Innovation and Technology as a Power Electronics Control Engineer for renewable energy applications. From 2014 to 2016, he was a Postdoctoral Researcher with the Department of Energy Technology, Aalborg University. Since 2016, he has been a Scientific Collaborator with the Power Electronics Laboratory, École Polytechnique Fédérale de Lausanne, Lausanne, Switzerland. His main research interests include power conversion technologies.

Drazen Dujic (S'03–M'09–SM'12) received the Dipl.-Ing. and M.Sc. degrees from the University of Novi Sad, Novi Sad, Serbia, in 2002 and 2005, respectively, and the Ph.D. degree from Liverpool John Moores University, Liverpool, U.K., in 2008, all in electrical engineering.

From 2002 to 2006, he was a Research Assistant with the Department of Electrical Engineering, University of Novi Sad. From 2006 to 2009, he was a Research Associate with Liverpool John Moores University. From 2009 to 2013, he was with the ABB Corporate Research Centre, Switzerland, as a Principal Scientist working on power electronics projects spanning the range from low-voltage/power switched-mode power supply in the below kilowatt range to medium-voltage high-power converters in the megawatt range. During 2010–2011, he was a member of a project team responsible for the development of the world's first power electronic traction transformer successfully commissioned on a locomotive. From 2013 to 2014, he was with ABB Medium Voltage Drives, Turgi, Switzerland, as an R&D Platform Manager, responsible for ABB's largest integrated-gate commutated-thyristor-based medium-voltage drive—ACS6000. He is currently an Assistant Professor with the École Polytechnique Fédérale de Lausanne, Lausanne, Switzerland, where he is also the Director of the Power Electronics Laboratory. He has authored or coauthored more than 80 scientific publications and has filed 11 patents. His current research interests include the areas of design and control of advanced high-power electronics systems and high-performance drives.

Dr. Dujic is an Associate Editor for the IEEE TRANSACTIONS ON INDUSTRIAL ELECTRONICS, IEEE TRANSACTIONS ON POWER ELECTRONICS, and *IET Electric Power Applications*. He received the First Prize Paper Award form the Electrical Machines Committee of the IEEE Industrial Electronics Society at the Annual Conference of the IEEE Industrial Electronics Society in 2007. In 2014, he received the Isao Takahashi Power Electronics Award for outstanding achievement in power electronics.

Wim van der Merwe (M'03-SM'14) received the B.Eng., M.Sc. (Eng), and Ph.D. degrees in electrical engineering from the University of Stellenbosch, Stellenbosch, South Africa, in 2000, 2006, and 2011, respectively.

He joined ABB Corporate Research in 2012 and is currently R&D Platform Manager of the ACS6000 MV-drive at ABB Medium Voltage Drives in Turgi, Switzerland. His research interests include multilevel and medium-voltage power electronic converters and the modeling of complex power electronic systems.